

Preprint notes:

This is a preprint of a letter to the editor recently submitted to the Journal of Theoretical Biology. Additional notices will be posted here if the letter is accepted for publication, including a full link to the finalized, accepted version at the publisher's website.

Improved patient-specific calibration for agent-based cancer modeling

Alice Hyun and Paul Macklin*

* Corresponding author: Paul.Macklin@usc.edu

URL: http://www.mathcancer.org/Publications.php#macklin12a_itb

Supplementary data: http://www.MathCancer.org/JTB_DCIS_2012/

BibTeX Citation:

```
@article{macklin12a_jtb,  
  author="Hyun, Alice and Macklin, Paul",  
  title="Improved patient-specific calibration for agent-based cancer modeling",  
  journal="J. Theor. Biol.",  
  year="2012",  
  note="(in review)",  
  URL="http://MathCancer.org/Publications.php#macklin12a_jtb ",  
}
```

EndNote Citation: http://www.mathcancer.org/RIS_journal.php?key=macklin12a_itb&file=xml_data/journal_articles.xml

Letter to the editor:

Improved patient-specific calibration for agent-based cancer modeling

Alice Hyun¹ and Paul Macklin^{1,2}

Refers to Macklin et al., *Journal of Theoretical Biology*, Volume 301, 21 May 2012, Pages 122-140. DOI: 10.1016/j.jtbi.2012.02.002

Macklin et al. (2012) recently introduced a mechanistic agent-based cell model, with application to ductal carcinoma in situ (DCIS)—a precursor to invasive breast cancer. The work included the first patient-specific calibration method to use pathology data from a single time point, as might be expected in a pre-surgical biopsy. The key measurements included the proliferative index (PI: the percentage of cycling cells), the apoptotic index (AI: the percentage of cells apoptosing), the mean viable rim thickness $\langle T \rangle$, the mean duct radius $\langle R_{\text{duct}} \rangle$, the mean nuclear radius $\langle R_N \rangle$, mean cell density $\langle \rho \rangle$, and the cell confluence f (percentage of the viable rim occupied by cell mass).

The authors demonstrated the calibration for an individual patient with solid-type DCIS with comedonecrosis, and used the calibrated model to predict the patient's DCIS growth rate and pathology-mammography size correlations. While the model predictions were quantitatively consistent with literature reports for similar cases, the calibration over-predicted the patient's proliferative index (PI), under-predicted the cell density, and over-predicted the patient's viable rim size. The authors attributed the discrepancy in PI to the neglect of the post-mitotic G_1 phase in the calibration method (daughter cells stain positive for Ki-67 after mitosis as they continue to cycle and grow, then exit to G_0), while they concluded that approximating the viable rim as 100% confluent likely caused the discrepancies in the cell density and viable rim size.

We now present and demonstrate an improved calibration method that addresses these shortcomings. We find that the new calibration substantially improves the model match to the patient's PI, AI, $\langle \rho \rangle$, and $\langle T \rangle$ measurements; this should make possible better quantitative model predictions of individual patients' tumor growth. In the interests of brevity, we only present the changes in the calibration. A MATLAB script is provided at MathCancer.org to help automate the calibration.

Population dynamics: Let PI_1 be the pre-mitotic cycling cells (S, G_2 , M, and possibly parts of G_1 , with duration τ_1), and let PI_2 be the cells in the post-mitotic G_1 phase (with duration $\tau_2 = \tau_{G_1}$). Let AI be as before, with duration τ_A . Note that $PI_1 + PI_2 = PI$ and $\tau_1 + \tau_2 = \tau_P$. PI_1 , PI_2 , and AI satisfy:

$$\dot{PI}_1 = \langle \alpha_P \rangle (1 - AI - PI) - \frac{1}{\tau_1} (PI_1 + PI_1^2) + \frac{1}{\tau_A} PI_1 \cdot AI \quad (1)$$

$$\dot{PI}_2 = \frac{2}{\tau_1} PI_1 - \frac{1}{\tau_2} PI_2 + \frac{1}{\tau_A} PI_1 \cdot AI \quad (2)$$

$$\dot{AI} = \alpha_A (1 - AI - PI) - \frac{1}{\tau_1} PI_1 \cdot AI - \frac{1}{\tau_A} (AI - AI^2). \quad (3)$$

As in Macklin et al. (2012), we assume a steady-state population dynamic and set \dot{PI}_1 , \dot{PI}_2 , and \dot{AI} equal to zero. Assuming we have measurements for AI, PI, τ_A , τ_1 , and τ_2 , we must solve for PI_1 (or PI_2), $\langle \alpha_P \rangle$, and α_A . Eqn. 2 can be explicitly rewritten to solve for PI_1 by substituting $PI_2 = PI - PI_1$. Hence:

$$PI_1 = \frac{\tau_1}{\tau_1 + 2\tau_2 + AI \frac{\tau_1 \tau_2}{\tau_A}} PI. \quad (4)$$

Using this, we can solve for $\langle \alpha_P \rangle$ and α_A :

$$\langle \alpha_P \rangle = \frac{\frac{1}{\tau_1} PI_1 (1 + PI_1) - \frac{1}{\tau_A} PI_1 \cdot AI}{1 - AI - PI} \quad (5)$$

$$\alpha_A = \frac{\frac{1}{\tau_A} (AI - AI^2) + \frac{1}{\tau_1} AI \cdot PI_1}{1 - AI - PI}. \quad (6)$$

The remainder is as in Macklin et al. (2012).

Cell geometry: We do not have quantitative measurements of the patient's confluence, but we estimate $f \sim 0.90$. We continue to set $\langle R_N \rangle = 5.295 \mu\text{m}$. If $\langle A \rangle$ is the mean cell cross-sectional area and $\langle R \rangle$ is the mean cell radius,

$$f = \langle \rho \rangle \langle A \rangle \approx \langle \rho \rangle \pi \langle R \rangle^2. \quad (7)$$

Next, we relate $\langle R \rangle$ to the quiescent cell radius \bar{R} via the AI, PI_1 and PI_2 fractions from above:

$$\langle V \rangle = \frac{4}{3} \pi \langle R \rangle^3 = PI_1 \langle V_1 \rangle + PI_2 \langle V_2 \rangle + AI \langle V_A \rangle + (1 - AI - PI) \langle V_Q \rangle, \quad (8)$$

where $\langle V_x \rangle$ is the mean cell volume in the x phenotypic state ($x \in \{\mathcal{P}_1, \mathcal{P}_2, \mathcal{A}, \mathcal{Q}\}$). For the model in Macklin et al. (2012),

$$\langle V_1 \rangle = \frac{4}{3} \pi \bar{R}^3, \quad \langle V_2 \rangle = \pi \bar{R}^3, \quad \langle V_A \rangle = \frac{4}{3} \pi \bar{R}^3, \quad \text{and} \quad \langle V_Q \rangle = \frac{4}{3} \pi \bar{R}^3. \quad (9)$$

Using these, we directly solve for \bar{R} and \bar{V} , the equivalent radius and cell volume in the quiescent state \mathcal{Q} . More detailed cell volume models (e.g., as in Mumenthaler et al. (2012)) require adjusting these per-state mean volumes.

Email address: Paul.Macklin@usc.edu (Paul Macklin).

URL: <http://www.MathCancer.org> (Paul Macklin).

¹ Center for Applied Molecular Medicine, Keck School of Medicine, University of Southern California, Los Angeles, CA, USA

² Corresponding author

Oxygen: We modify the oxygen equation such that oxygen is uptaken at rate λ in the confluent fraction of the viable rim, and at rate λ_b in the non-confluent portion of the rim. This gives a mean uptake rate of $\lambda_{\text{viable}} = f\lambda + (1-f)\lambda_b$ in the viable rim, and $\lambda_{\text{core}} = \lambda_b$ in the necrotic core. Define the length scales

$$L_V = \sqrt{D/\lambda_{\text{viable}}} = L_0/\sqrt{f + (1-f)\lambda_b/\lambda} \quad (10)$$

and

$$L_N = \sqrt{D/\lambda_{\text{core}}} = L_0/\sqrt{\lambda_b/\lambda}, \quad (11)$$

in the viable rim and necrotic core, respectively, where L_0 (100 μm) is the viable oxygen diffusion length scale. Define the mean necrotic core radius $\langle R_{\text{NC}} \rangle = \langle R_{\text{duct}} - T \rangle$. After adjusting the oxygen equations from Macklin et al. (2012) to use these uptake rates, solving analytically, and evaluating at the duct boundary, we find the updated oxygen boundary value σ_B via:

$$\frac{\sigma_B}{\sigma_H} = \cosh\left[\frac{\langle T \rangle}{L_V}\right] + \frac{L_V}{L_N} \tanh\left[\frac{R_{\text{NC}}}{L_N}\right] \sinh\left[\frac{\langle T \rangle}{L_V}\right]. \quad (12)$$

The mean oxygen in the viable rim is obtained via:

$$\frac{\langle \sigma \rangle}{\sigma_H} = \frac{L_V}{\langle T \rangle} \left[\sinh\left[\frac{\langle T \rangle}{L_V}\right] + \frac{L_V}{L_N} \tanh\left[\frac{R_{\text{NC}}}{L_N}\right] \left(\cosh\left[\frac{\langle T \rangle}{L_V}\right] - 1 \right) \right] \quad (13)$$

Cell-cell mechanics: For the general case where $f \neq 1$, we determine the mean cell-cell spacing s in the confluent region by

$$s = \sqrt{(2f)/(\sqrt{3}\langle \rho \rangle)} \quad (14)$$

The mechanics calibration continues as in Macklin et al. (2012) with this altered mean cell-cell spacing in the confluent region.

Updated parameter values: Using this updated calibration for the patient data presented in Macklin et al. (2012), the new patient-specific parameters are given in Table 1.

Parameter	Physical Meaning	Value
R	quiescent cell radius	9.536 μm
R_N	cell nuclear radius	5.295 μm
σ_B	oxygen value on the BM	0.257280
$\langle \sigma \rangle$	mean oxygen level in viable rim	0.218997
$\langle \alpha_P \rangle$	mean $\mathcal{Q} \rightarrow \mathcal{P}$ transition rate	0.00826266 h^{-1}
$\overline{\alpha_P}^{-1}$	mean waiting time prior to $\mathcal{Q} \rightarrow \mathcal{P}$ transition when $\sigma = 1$	172.43 min
α_A	$\mathcal{Q} \rightarrow \mathcal{A}$ transition rate	0.00123827 h^{-1}
s	cell spacing	17.985 μm
c_{cca}	cell-cell adhesive force coefficient	0.0489414 c_{CCR}
c_{cba}	cell-BM adhesive force coefficient	10 c_{cca}

Table 1

Updated patient-specific parameters for Patient 100019 for the DCIS model.

Comparison against the original calibration: We simulated 45 days of growth using the updated parameter values above. As in Macklin et al. (2012), we post-processed the original and new simulations in 1-hour increments to calculate the simulated PI, AI, cell density, and viable rim thickness. Further postprocessing details and open source C++ code can be found in Macklin et al. (2012) and at http://MathCancer.org/JTB_DCIS_2012/.

For each simulation, we calculated the mean and standard deviation of these statistics from T_{150} to 45 days. (T_{150} is the first time the ‘‘cropped’’ portion of the viable rim has at least 150 cells. This helps us to more directly compare the simulations while (1) eliminating early transient dynamics and (2) including at least

15 days of simulated data as in Macklin et al. (2012).) For the original simulation in Macklin et al. (2012), $T_{150} = 21.04$ days; for the new parameter values, $T_{150} = 29.29$ days.

In Fig. 1, we plot the means (triangles) of PI, AI, density, and viable rim size for the patient (red bars), original parameter values (blue), and new parameter values (black). The bars represent \pm one standard deviation of each quantity, to give a sense of the variability of each measurement. Our new calibration (black bars) is much more successful than our old calibration (blue bars) at matching the patient’s mean PI, density, and viable rim size. See Table 2.

Simulated statistics (left bars) vs. patient data (right bars)
(All bars are mean \pm standard deviation)

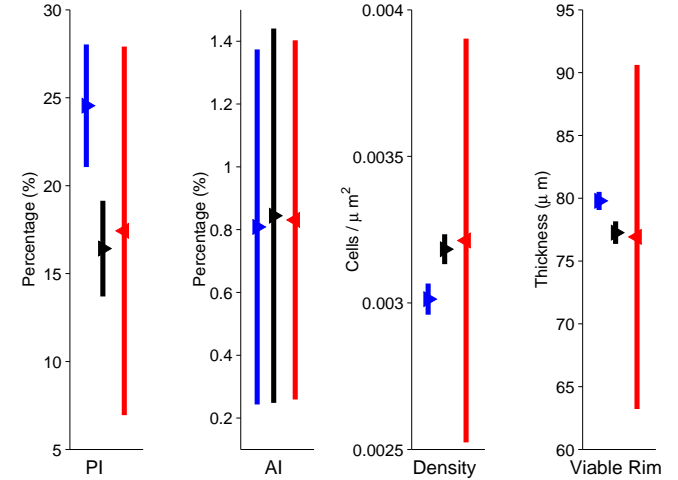


Fig. 1. Comparison of calibration methods: We compare the simulated (left bars) and patient (right bars) PI (column one), AI (column two), cell density (column three), and viable rim thickness (column four) for our original calibration method (left blue bars) and the improved calibration (middle black bars), from T_{150} to 45 days in our simulations. While the original calibration (left blue bars) was consistent with the patient data (right red bars), the new calibration (middle black bars) gives simulated means that match the patient data much more closely.

Quantity	Patient Data	New Calibration	Old Calibration
PI (%)	17.43 \pm 9.25	16.42 \pm 2.72	24.55 \pm 3.49
Corrected AI (%)	0.831 \pm 0.572	0.844 \pm 0.596	0.809 \pm 0.565
Cell density (cells/ μm^2)	3.213e-3 \pm 5.95e-4	3.183e-3 \pm 5.09e-5	3.013e-3 \pm 5.30e-5
Viable rim thickness (μm)	76.92 \pm 12.51	77.26 \pm 0.90	79.79 \pm 0.72

All measurements given as mean \pm standard deviation

Table 2

Verification of the patient-specific calibration: Comparison of the patient (second column) and computed (third and fourth columns) mean and standard deviation for the proliferative index, apoptotic index, cell density, and viable rim thickness. All computed quantities are within the range of patient variation; the new calibration (third column) is substantially better than the original (fourth column).

Final thoughts: As suggested in Macklin et al. (2012), agent-based model calibration to individual patients can be substantially improved by accounting for (1) post-mitotic Ki-67 positive cells in the G_1 phase, and (2) the viable rim cell confluence. In our tests, the new calibration better matches the patient’s PI, density, and viable rim size. In continuing work, we are applying this new calibration to a larger number of patients for a case-by-case validation of personalized predictions of cancer progression.

Acknowledgements: PM and AH thank the USC Center for Applied Molecular Medicine for generous computational resources; we thank the USC Undergraduate Research Associates Program (URAP) for support. PM thanks the National Institutes of Health for the Physical Sciences Oncology Center grant 5U54CA143907 for Multi-scale Complex Systems Transdisciplinary Analysis of Response to Therapy (MC-START), and the

USC James H. Zumberge Research and Innovation Fund (2012 Large Interdisciplinary Award) for support through the Consortium for Integrative Computational Oncology (CICO).

References

- P. Macklin, M. E. Edgerton, A. M. Thompson, and V. Cristini. Patient-calibrated agent-based modelling of ductal carcinoma in situ (DCIS): From microscopic measurements to macroscopic predictions of clinical progression. *J. Theor. Biol.*, 301:122–40, 2012. doi: 10.1016/j.jtbi.2012.02.002.
- S. Mumenthaler, A. Hyun, and P. Macklin. Integrative experimental-computational modeling of intracellular water transport and solid synthesis in breast cancer cells: implications for patient-specific simulation of ductal carcinoma in situ (DCIS). *Phys. Biol.*, 2012. (in preparation).